



# Shedding light on the photocatalytic hydrogen generation from seawater using CdS

Deva Pelayo, Eduardo Pérez-Peña, María J. Rivero, Inmaculada Ortiz\*

Departamento de Ingenierías Química y Biomolecular, Universidad de Cantabria, Avda. Los Castros, s/n, Santander 39005, Spain

## ARTICLE INFO

### Keywords:

hydrogen generation  
photocatalysis  
seawater  
CdS  
TiO<sub>2</sub>

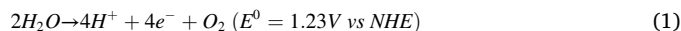
## ABSTRACT

The current energy crisis, in addition to the severe drought our planet is suffering, had led to the search for new alternatives to obtain green and sustainable fuel sources. Green hydrogen as an energy vector is one of the most promising possibilities. In this context, emerging technologies, such as photocatalysis, that can be driven by solar light, become especially challenging when using natural seawater (NSW) directly, avoiding previous purification steps. The exploitation of this endless resource is key to tackle the climate and energy emergency, although it faces questions derived from the presence of dissolved salts at significant concentrations. So far, some reports attribute to the latter the catalyst deactivation and loss of performance, whereas other authors have compared the results obtained with NSW and synthetic seawater and have reported higher rates of hydrogen generation with NSW. To solve this controversy, further research is needed to assess both the viability of the photocatalytic hydrogen generation from NSW and the conditions for the optimum process performance. Within this context, this study has evaluated two easy to purchase photocatalysts, TiO<sub>2</sub> as benchmark, and CdS, in a concentration range from 50 to 150 mg L<sup>-1</sup>. Different sacrificial agents are used depending on the catalyst, 20% CH<sub>3</sub>OH for TiO<sub>2</sub> and 0–0.1 mol L<sup>-1</sup> Na<sub>2</sub>S/Na<sub>2</sub>SO<sub>3</sub> range for CdS. The experiments performed in batch mode gave promising results and shed new light on the positive influence of the buffer capacity of NSW, providing information about the mechanisms that take place during the process. Furthermore, this study fosters the advancement of hydrogen production technologies based on abundant and inexpensive raw materials.

## 1. Introduction

With the relentless rise in global energy demand, the need for clean and renewable fuel sources has become more apparent than ever. The search for sustainable alternatives to meet these growing requirements has led to exhaustive research on innovative technologies. In this context, hydrogen has emerged as energy carrier and a promising alternative due to its high efficiency properties and eco-friendly nature [1–4], making it a potential game-changer in the transition to a greener future. The versatility of hydrogen as energy carrier and its potential to decarbonize various sectors has generated vast interest and motivated extensive research on various hydrogen production technologies [5–7]. Several methods have been developed to produce hydrogen. Although conventional approaches are promising, their dependence on fossil fuels or high energy consumption increases concerns about their long-term

sustainability and environmental impact [8]. To the contrary, since the discovery of photocatalytic water splitting with TiO<sub>2</sub> [9], photocatalytic hydrogen production, although at a low scale, offers a compelling and sustainable alternative that harnesses the power of visible light to drive the water splitting reaction, releasing hydrogen and oxygen that is the only by-product (Eqs. (1)–(2)) [10–15].



This reaction of water decomposition into H<sub>2</sub> and O<sub>2</sub> (Eq. (1)) is an endothermic process with a Gibbs free energy of 237 kJ mol<sup>-1</sup>. It also requires a potential of 1.23 eV to oxidize the water molecule and therefore a photocatalyst to generate enough potential for the reaction to occur (Eq. (3)). Hence, the band gap of the semiconductor

*Abbreviations:* CDs, Carbon dots; D.L, Detection limit; EDS, Energy dispersive spectroscopy; HPR, Hydrogen production rate; IEP, Isoelectric point; NHE, Normal Hydrogen Electrode; NSW, Natural seawater; SEM, Scanning electron microscopy; SSW, Synthetic seawater; TCD, Thermal conductivity detector; UP, Ultrapure water; XPS, X-ray photoelectron spectroscopy.

\* Corresponding author.

E-mail address: [ortizi@unican.es](mailto:ortizi@unican.es) (I. Ortiz).

<https://doi.org/10.1016/j.cattod.2024.114672>

Received 18 October 2023; Received in revised form 4 January 2024; Accepted 25 March 2024

Available online 29 March 2024

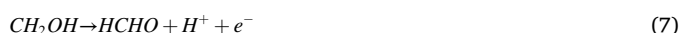
0920-5861/© 2024 The Authors. Published by Elsevier B.V. This is an open access article under the CC BY-NC-ND license (<http://creativecommons.org/licenses/by-nc-nd/4.0/>).

photocatalyst must be greater than 1.23 eV (<1000 nm) and less than 3.0 eV (>400 nm) to be operated under visible light and harness available solar light [16,17]. In particular, the energy level of the catalyst's conduction band (CB) should be more negative than the  $H^+/H_2$  reduction potential of Eq. (2) to produce hydrogen from water. When the valence band (VB) energy level is more positive than the  $H_2O/O_2$  oxidation potential from Eq. (1), oxygen can also be produced from water. However, some semiconductors are more susceptible to photocorrosion rather than  $O_2$  generation. For example, the oxidation of water to form oxygen is not possible when working with cadmium sulfide (CdS), because the  $S^{2-}$  anion is more susceptible to oxidation than water [18].

When the semiconductor absorbs sufficient energy to overcome the band gap, the electrons ( $e^-$ ) from the VB migrate to the CB, leaving holes ( $h^+$ ) in the VB, (Eq. (3)) [14,15]. Then, the electrons contribute to the photocatalytic water splitting (Eq. (4)) [18].



The hydrogen production via water splitting using  $TiO_2$  semiconductor photocatalyst has been widely studied because of its simplicity of operation and significant results. For instance, DeepanPrakash et al. [19] obtained  $6.1 \cdot 10^4 \mu\text{mol h}^{-1} \text{g}_{\text{cat}}^{-1}$  with  $TiO_2$  in 30 minutes. Nevertheless,  $TiO_2$  has a wide band gap (3.2 eV approximately), with a conduction band potential of ca.  $-0.3$  V and a valence band potential of ca. 3.0 V (vs. NHE at pH = 0) [14,15,20], which allows light to be absorbed only in the ultraviolet spectrum, making its efficiency under solar light limited, as sunlight only contains less than 5% of ultraviolet wavelength [21,22]. The band gap value of  $TiO_2$  was calculated using the Tauc method based on the optical absorption spectrum [23]. Another drawback is the fast electron-hole recombination of  $TiO_2$ , reducing its hydrogen evolution rate [24]. Therefore, subsequent studies synthesized composites with  $TiO_2$  and other photocatalysts or used some co-catalysts to be active in the visible wavelength and improve the hydrogen production rate, HPR. Gao et al. [25] developed  $SiO_2/Ag@TiO_2$  core-shell nanocomposites, reaching a HPR of  $1.5 \cdot 10^3 \mu\text{mol h}^{-1} \text{g}_{\text{cat}}^{-1}$  in a solar thermal collector. Guo et al. [26] fabricated  $MoS_2@TiO_2$ , which achieved a HPR of  $2.0 \cdot 10^5 \mu\text{mol h}^{-1} \text{g}_{\text{cat}}^{-1}$  under visible light. When  $TiO_2$  is used, sacrificial agents with alcohol groups need to be present to prevent some of the fast charge recombination, even when heterojunctions or co-catalysts are used, to enhance the photocatalytic efficiency. The alcohol groups are needed because as the catalyst is an oxide, it needs to replace the OH groups. To this end, methanol has been widely used [10,27–30], but other alcohols such as glycerol [28] have been also used in previous studies. Working with methanol as sacrificial agent in the experiments with  $TiO_2$ , the reactions that take place in the medium are detailed below, Eq. (5) to Eq. (9), with Eq. (10) being the overall reaction [28].

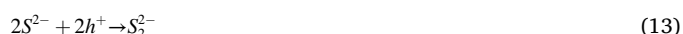


Even though composites and co-catalysts have demonstrated competent performance at lab-scale, for the future deployment and process scale-up it is key to consider commercially available, cost-effective and environmentally sustainable photocatalysts active under visible light.

CdS is one of the best materials used so far for the photocatalytic production of  $H_2$  under visible light along with other applications [31, 32]. It has a narrow band gap of 2.4 eV (512 nm of wavelength) [13], with ca.  $-0.5$  V vs NHE of conduction band potential and ca. 1.7 V vs NHE of valence band potential [14,15,20]. The band gap value was determined using the Tauc method in the same way as for  $TiO_2$  [33]. The high activity of CdS has been attributed to its crystal structure, specific surface area and particle size, which can also be modified to improve the HPR [8]. Although limited by its photocorrosion and rapid recombination of photogenerated electron-hole pairs, there are strategies to inhibit these effects. In recent years, interesting reviews about photocatalytic hydrogen production have been published collecting the best improvements and future perspectives on the topic. Most of them have focused on heterojunctions of CdS with different semiconductors to improve the photocatalytic efficiency and stability of the materials [14,15,31, 34–39]. For instance, Li et al. [31] reported improvements in the HPR of more than 8-fold with CdS-MoS<sub>2</sub> with respect to CdS. Zhang et al. [15] compiled the main advances achieved with heterostructures and synthesis methods to improve hydrogen productions; they reported a 28-fold improvement with CdS/ZnS relative to CdS.

However, to shed light on the photocatalytic hydrogen production with bare CdS (without the addition of another semiconductor) the use of a sacrificial agent can mitigate the photo-corrosion effect as well as increase its efficiency [16]. Most of the previous studies with CdS or its composites used  $Na_2S/Na_2SO_3$  as sacrificial agent [40–44], but alcohols [45] or lactic acid [46] have been employed as well. The  $Na_2S/Na_2SO_3$  combination appears as the most appropriate reagent for regenerating CdS, because when  $Na_2S$  partially dissociates in water,  $S^{2-}$  and  $HS^-$  are formed, and the photocatalyst holes oxidize  $Na_2S$  avoiding photocorrosion of the catalyst [28,29].

Eqs. (11)–(17) show the effect of the sacrificial agent  $Na_2S/Na_2SO_3$  on the photocatalyst, where two holes are involved, corresponding to the two electrons of Eq. (4). First,  $Na_2S$ , the hole scavenger, is dissociated in the aqueous solution (Eq. (11)) into  $S^{2-}$ , which subsequently forms  $S_2^{2-}$  and  $HS^-$  (Eqs. (12)–(13)).  $S_2^{2-}$  is an optical filter that may hinder hydrogen production by competing with the main reaction of water splitting [18]. Because of this effect,  $Na_2SO_3$  is added to the sacrificial agent pair, that helps capture more holes. When  $Na_2SO_3$  is dissolved in water, it forms  $SO_3^{2-}$ , which enables the conversion of  $S_2^{2-}$  back to  $S^{2-}$  (Eqs. (14)–(16)). Additionally, the presence of thiosulfate can prevent sulfur deposition on the catalyst, which could lead to its deactivation. Then, the overall reaction of water splitting in presence of the sacrificial agent  $Na_2S/Na_2SO_3$  is summarized in Eq. (17) [18]. It is worth noting that when using a hole scavenger, the mechanism leading to hydrogen generation is given by reactions (11)–(17), that substitute reaction (1) to (12) [8].



Chang et al. [47] found that pH = 9.0 was the optimal pH value for the reaction of water splitting with CdS and  $Na_2S/Na_2SO_3$  as sacrificial agent, out of the experimental values of pH: 3, 6, 9, 12. This phenomenon was attributed to the increased dissociation of  $HS^-$  and  $S^{2-}$  at higher pH values ( $pK_{a,Na_2S} = 3.09$  [48]). However, excessive hydroxide ions at extreme alkaline pH can react with the hydrogen ions to form water,

thus reducing the hydrogen production efficiency [47].

Specifically, the use of seawater as the reaction medium in photocatalytic hydrogen production is key for further implementation. Seawater is abundant and readily available, although a priori, the presence of ionic components and impurities could affect the stability of the hydrogen production process. So far, only a few studies have evaluated the use of natural seawater for the photocatalytic water splitting with photocatalysts such as Pt-CdS/TiO<sub>2</sub>, SiO<sub>2</sub>/Ag@TiO<sub>2</sub>, Pt/TiO<sub>2</sub>, Pt-organic-C<sub>3</sub>N<sub>4</sub>, CDs/CdS, TiO<sub>2</sub>/Pt/Cd<sub>0.8</sub>Zn<sub>0.2</sub>S, and ZnO/Pt/Cd<sub>0.8</sub>Zn<sub>0.2</sub>S [25,46,49–52] (Table S.1). For instance, Zhu et al. [46] used CdS with carbon dots (CDs) and lactic acid as sacrificial reagent in the photocatalysis of natural seawater and reported worse results compared to ultrapure water. A similar trend was observed by other authors, such as Ayyub et al. [52] with TiO<sub>2</sub>/Pt/Cd<sub>0.8</sub>Zn<sub>0.2</sub>S, and ZnO/Pt/Cd<sub>0.8</sub>Zn<sub>0.2</sub>S composites using benzyl alcohol/acetic acid as sacrificial agent. In the work of Ji et al. [49], the hydrogen production results are slightly improved when natural seawater is used compared to ultrapure water experiments, Pt/CdS/TiO<sub>2</sub> composite as photocatalyst and Na<sub>2</sub>S/Na<sub>2</sub>SO<sub>3</sub> as sacrificial agent. As shown in Table S.1, most of published works used complex composites or co-catalysts to achieve satisfactory results, that required complex synthesis, high cost and low environmental sustainability. In addition, inconsistent results have been reported regarding the use of natural seawater (NSW) for hydrogen production by photocatalysis. In this article, to shed light on the phenomena involved in the photocatalytic water splitting using CdS as photocatalyst, experiments with different water media, synthetic seawater, SSW, with different NaCl concentrations (0–35 g L<sup>-1</sup>), and NSW have been performed with photocatalyst concentrations from 25 to 150 mg L<sup>-1</sup> and sacrificial agent concentrations from 0 to 0.1 mol L<sup>-1</sup>.

## 2. Materials and methods

### 2.1. Materials

Sodium sulfide hydrate (Na<sub>2</sub>S·xH<sub>2</sub>O), cadmium chloride hemi(pentahydrate) (CdCl<sub>2</sub>·2 ½ H<sub>2</sub>O), and thiourea (CH<sub>4</sub>N<sub>2</sub>S) were purchased from Sigma-Aldrich. Sodium sulfite anhydrous (Na<sub>2</sub>SO<sub>3</sub>) 98+ % was provided by Thermo Scientific. Titanium dioxide (TiO<sub>2</sub>) Aeroxide® P25 was supplied by Evonik Degussa. Commercial CdS nanoparticles were provided by Chemazone. Nevertheless, to assess the influence of the impurities of the commercial product, CdS particles were also synthesized in our laboratory. Sodium chloride (NaCl) 99.5% and pure methanol (CH<sub>3</sub>OH) from Fisher Scientific were used. Pure argon (Ar) was purchased from Nippon Gases.

### 2.2. Synthesis of CdS

CdS photocatalyst was prepared by a hydrothermal method. First, 0.13 M of CdCl<sub>2</sub> was stirred in a water solution for 10 min. Then, an aqueous solution of 0.73 M of CH<sub>4</sub>N<sub>2</sub>S was added to the previous solution and stirred for 1 h. Later, the mixture was transferred to a 50 mL Teflon autoclave, sealed, and heated at 180°C for 24 h. After the autoclave was cooled to room temperature, the product was collected and washed three times with deionized water and two times with ethanol and centrifuged for 3 min. Finally, it was dried at 80°C for 12 h.

### 2.3. Photocatalysts characterization

The photocatalyst morphology was studied by scanning electron microscopy (SEM) using a Carl Zeiss, model EVO MA 15 microscope, implemented with energy dispersive spectroscopy (EDS) microanalysis system from the brand Oxford. Raman spectra were obtained using a Jasco 4500 spectrophotometer equipped with a green diode laser excitation source (531.9 nm). X-ray photoelectron spectroscopy (XPS) was performed in a XPS Spectrometer Kratos AXIS Supra obtained from a monochromatic Al K $\alpha$  source applying 15 kV and 75 W. Zeta potential of

the photocatalyst particles was measured in a Zetasizer Nano ZS from Malvern at pH range 2–12. The hydroxyl radical quantification was performed following the methodology described by Tai et al. [53].

### 2.4. Photocatalytic activity

The photocatalytic activity was assessed with different aqueous media that contained the photocatalyst and the sacrificial agent in absence of air, that were continuously stirred. The photocatalysts studied were TiO<sub>2</sub> and CdS. TiO<sub>2</sub>, that has well-established photocatalytic properties and extensive literature data, has been experimentally tested to provide a reliable benchmark and ensure a consistent and rigorous evaluation of the photocatalytic generation of hydrogen from seawater. Different sacrificial agents have been used according to the catalysts, CH<sub>3</sub>OH for TiO<sub>2</sub> and Na<sub>2</sub>S/Na<sub>2</sub>SO<sub>3</sub> for CdS. The aqueous media evaluated were ultra-pure water (UP) with 18.2 M $\Omega$ .cm of resistivity, SSW which is a 35 g L<sup>-1</sup> NaCl solution, and NSW. The photocatalytic experiments were carried out in a lab-scale photo-reactor (Apria Systems, S. L.) operating in batch mode. It is a cylindrical borosilicate glass flask with a capacity of 300 mL and it is provided with two outlets to allow sample collection and argon inertization, which is performed prior to the photocatalytic experiment. The photo-reactor has an illuminated surface of 290 cm<sup>2</sup>, and the gas volume is 50 mL. It is surrounded by four fluorescent lamps (UV or visible, depending on the catalyst used) arranged in a cross pattern (Fig. 1). The UV lamps, with 12.5 W m<sup>-2</sup> irradiance each and 9 W of power consumption, were purchased from Philips. The visible lamps have 48.3 W m<sup>-2</sup> of irradiance, 9 W, and they were purchased from Osram Dulux®.

The experimental time was 24 h, and every hour gas aliquots were taken from the top of the photo-reactor with a 2.5 mL syringe with PTFE plunger tip and removable luer-lock needle, purchased from Agilent. The hydrogen production was measured in a gas chromatograph GC-2010 Plus provided with thermal conductivity detector (TCD) from Shimadzu, with a Shin Carbon ST 80/100 column and a detection limit of 7.5  $\mu$ mol using argon as a carrier gas. All experiments were performed in duplicate, and the average values with standard deviations are reported.

## 3. Results and discussion

### 3.1. Hydrogen generation from synthetic seawater (SSW)

The performance of the synthesized CdS was compared with the commercial semiconductor. Figure S.1 shows the hydrogen production using commercial CdS nanoparticles and those synthesized in the laboratory by the hydrothermal method. The results are very similar; therefore, the experimental analysis was done with the synthesized material for economic reasons.

In Figure S.2, SEM images showed a feather-like morphology of the synthesized CdS, with a particle size of 4–8  $\mu$ m, slightly bigger than

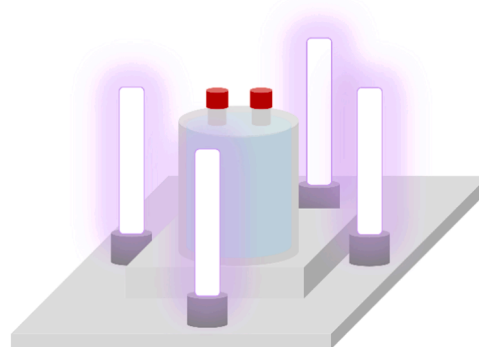


Fig. 1. Lab-scale photo-reactor.

other CdS feathers-like shapes reported in the literature [54,55]. This difference is attributed to the synthesis method. The porous structure of CdS with feather-like morphology and 3  $\mu\text{m}$  of particle size was analyzed by Bajorowicz et al. [54] achieving  $1.2 \text{ m}^2 \text{ g}^{-1}$  of BET surface area and  $0.0006 \text{ cm}^3 \text{ g}^{-1}$  of pore volume. EDS spectroscopy was used to evaluate the homogeneity of Cd and S in the synthesized CdS, which is confirmed in Figure S.2d-e, no impurities were observed in the material. On the other hand, SEM and EDS analysis revealed heterogeneous morphology of commercial CdS, with a mixture of CdS nanoparticles and  $\text{SiO}_2$  particles of 10–12  $\mu\text{m}$  (Figure S.3). This can be observed in the Raman spectra as well, with the two characteristic peaks of CdS at 300 and 600  $\text{cm}^{-1}$  in the synthesized CdS, whereas the commercial particles showed a third peak at 450  $\text{cm}^{-1}$ , which corresponds to  $\text{SiO}_2$  (Figure S.4). Moreover, the presence of these impurities supported the selection of the synthesized CdS in the experiments of hydrogen production.

Some gas samples from the experiments were analyzed in a micro gas chromatograph (micro-GC 990) with a MS5A SS column, purchased from Agilent, calibrated to measure the concentration of  $\text{H}_2$ ,  $\text{O}_2+\text{N}_2$ ,  $\text{CO}$ ,  $\text{CH}_4$ , and  $\text{CO}_2$ . As the aliquots only showed hydrogen and air (the combination of  $\text{O}_2$  and  $\text{N}_2$ ) peaks, in the following experiments all the samples were measured in the gas chromatograph GC-2010 Plus from Section 2.4.

Preliminary experiments were carried out with SSW and  $\text{TiO}_2$  by systematically varying the NaCl concentration from 0  $\text{g L}^{-1}$  to 35  $\text{g L}^{-1}$ , the salt concentration of NSW, detailed in Fig. 2. These experiments were carried out with 170  $\text{mg L}^{-1}$  of  $\text{TiO}_2$  (catalyst concentration based on previous results) [30]. It was revealed that as the NaCl concentration increased a slight reduction on hydrogen production took place; overall the HPR remained in the range from 7 to 10  $\mu\text{mol h}^{-1} \text{ g}_{\text{cat}}^{-1}$ , Fig. 2. These results agree with previous data reported in literature working with  $\text{TiO}_2$  and SSW with different NaCl concentrations (0  $\text{g L}^{-1}$  and 35  $\text{g L}^{-1}$ ) [19, 56,57].

Fig. 3 delves into the influence of NaCl concentration on SSW splitting using CdS with a concentration from 50 to 150  $\text{mg L}^{-1}$ , to discern distinctive kinetics and ascertain its difference from  $\text{TiO}_2$ . It was revealed that photocatalysis was favored at lower concentrations of NaCl in SSW for CdS due to the interference of NaCl with the catalyst and the sacrificial agent  $\text{Na}_2\text{S}/\text{Na}_2\text{SO}_3$ . The sacrificial agent forms  $\text{Na}_2\text{O}$ , that turns into  $\text{NaOH}$  in aqueous solution, which causes an increase in pH up to  $13.0 \pm 0.2$  and a decrease in the hydrogen production rate. Figure S.5 shows the XPS spectra of CdS in different media, and Figure S.6 to S.9 show the deconvolutions of XPS spectra of synthesized CdS in different aqueous media. These figures illustrate the most probable states and bonds of each element. Figure S.6 shows the deconvolutions of synthesized CdS prior to be used: Cd 3d and S 2p. Both peaks of Figure S.6a, at 412.1 and 405.4 eV, are the typical signals for  $\text{Cd}^{2+}$  state in hexagonal CdS, Cd 3d<sub>5/2</sub> and Cd 3d<sub>3/2</sub> [59–62]. In Figure S.6b, both peaks, at 162.3 and 161.2 eV, are typical signals for  $\text{S}^{2-}$  state of CdS, S 2p<sub>1/2</sub>, and S 2p<sub>3/2</sub>

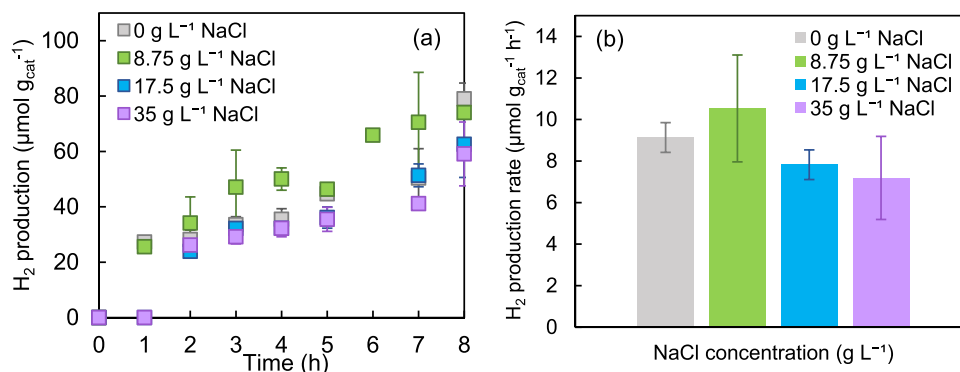


Fig. 2. Influence of NaCl concentration in the hydrogen production with SSW, 170  $\text{mg L}^{-1}$  of  $\text{TiO}_2$ , 20% of methanol and UV radiation ( $12.5 \text{ W m}^{-2}$ ), with a pH value of  $5.9 \pm 0.2$ . (a) Hydrogen production during the first 8 h of experiment, and (b) hydrogen production rate.

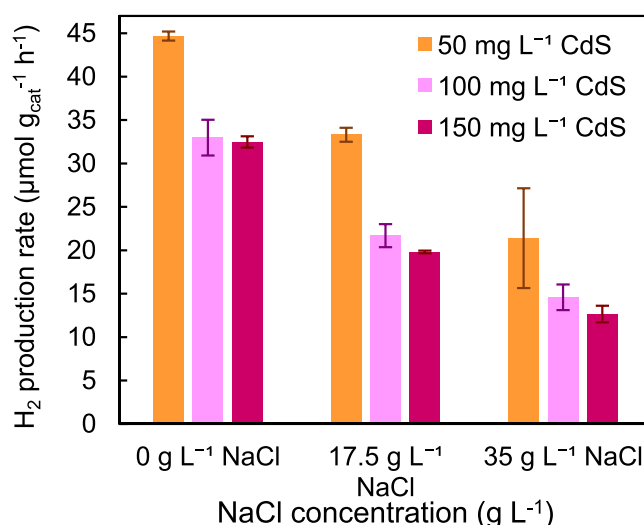


Fig. 3. Influence of NaCl concentration and catalyst concentration in the hydrogen production in SSW with visible light ( $48.3 \text{ W m}^{-2}$ ) and 0.1 M of  $\text{Na}_2\text{S}/\text{Na}_2\text{SO}_3$ , with a pH value of  $12.7 \pm 0.2$ .

[58,61–63]. Regarding Figure S.7, the CdS had been used in an experiment with UP water and the sacrificial agent ( $\text{Na}_2\text{S}/\text{Na}_2\text{SO}_3$ ) and, thus, Figure S.7c shows Na 1 s spectra, at 1071 eV, the characteristic energy for  $\text{Na}_2\text{SO}_4$  [64]. Moreover, Figure S.7b displays the same spectra of S 2p as Figure S.6b but two small peaks appear at 167.8 and 169.0 eV, which correspond to  $\text{SO}_3^{2-}$  and  $\text{SO}_4^{2-}$ , respectively [65]. This same spectrum is obtained with the synthesized CdS used with SSW and the sacrificial agent (Figure S.8), with the only difference of a new small peak at 1072.2 eV, corresponding to  $\text{Na}_2\text{O}$  [66]. As previously mentioned,  $\text{Na}_2\text{O}$  in aqueous media forms  $\text{NaOH}$ , increasing the pH to  $12.7 \pm 0.2$ . Even though alkaline pHs are beneficial for the water splitting reaction, this extreme alkaline pH is detrimental for the hydrogen production, because excessive hydroxide ions can react with hydrogen ions from water splitting [47].

Comparison of the results represented in Figs. 2 and 3 reveal the detrimental influence of the concentration of NaCl for both photocatalysts, being more pronounced when using CdS although this material is more effective in the production of hydrogen. Influence of NaCl on the  $\text{TiO}_2$  can be explained by the superficial charges of the photocatalyst, as represented by the zeta potential in Figure S.10. The  $\text{TiO}_2$  solution with methanol as sacrificial agent has an initial pH value of  $5.9 \pm 0.2$ , and as can be observed in Figure S.10, the  $\text{TiO}_2$  surface is positively charged at the studied pH value. Therefore, chloride anions can be electrostatically attracted by the catalyst [67], acting as hole scavenger, contributing to a better performance of the process [3], when low NaCl

concentrations are used, as observed in Fig. 2. Nevertheless, at higher NaCl concentrations, an inhibition effect may occur, since chloride ions might be adsorbed on the surface of the catalyst, occupying the active sites where the sacrificial agent acts. Considering this issue, the most probable mechanism of inhibition is due to the competition of two active species, sacrificial agent and photocatalyst [67]. DeepanPrakash et al. [19] observed a similar trend, with a 1.6-fold improvement when SSW was used. And Guo et al. [26] observed similar hydrogen production of about  $10 \mu\text{mol h}^{-1}$ . On the other hand, the suspension of CdS with  $\text{Na}_2\text{S}/\text{Na}_2\text{SO}_3$  has an initial pH value of  $12.7 \pm 0.2$ , and the catalyst is negatively charged (Figure S.10). Hence, chloride anions cannot be electrostatically attracted by the surface of CdS. Similar trend was also reported by other authors [21,46,68]. For instance, Liu et al. [21] observed a 1.5-fold improvement when working with pure water with respect to SSW for CdS, with maximum production of  $300 \mu\text{mol g}_{\text{cat}}^{-1}$ .

### 3.2. Hydrogen generation from natural seawater (NSW) photocatalytic splitting

Subsequently, a comprehensive evaluation of the real-world potential of the photocatalytic system was carried out by assessing its performance with NSW under similar conditions previously studied with SSW. The NSW ionic characterization is detailed in Table S.2. Fig. 4 below reveals the high photocatalytic potential for hydrogen production with NSW for both high concentrations of  $\text{TiO}_2$  and CdS semiconductors. It can be noted that y-axis of Fig. 4b is 2-fold the y-axis of Fig. 4a.

Furthermore, it is noteworthy that in the blank experiments carried out without catalyst ( $\text{TiO}_2$  or CdS), without sacrificial agent ( $\text{CH}_3\text{OH}$  or  $\text{Na}_2\text{S}/\text{Na}_2\text{SO}_3$ ), or without light (ultraviolet or visible), no hydrogen production was observed, or it was below the detection limit (D.L.) of  $7.5 \cdot 10^{-3} \mu\text{mol}$ .

The transition from SSW to NSW as the reaction medium in our photocatalytic hydrogen production experiments yielded a significant leap in performance. The utilization of NSW, with its complex matrix of salts and dissolved ions, enabled a more accurate representation of environmental factors faced in practical applications. The use of NSW could affect the stability of the hydrogen production process due to the presence of ionic components, as observed in Figure S.5 and S.9, where XPS spectra of synthesized CdS after experiments with NSW and  $\text{Na}_2\text{S}/\text{Na}_2\text{SO}_3$  are detailed. It reveals the effect of NSW with the sacrificial agent on the surface of the catalyst, which appears with interferences: Cd 3d and S 2p spectra are distorted. Na 1s and Mg 2p spectra are seen clearer as they are on the surface of the semiconductor, which may be detrimental to the seawater splitting as they could potentially block the active sites of the photocatalysts [3]. Figure S.9c depicts a similar

spectrum to Figure S.8c, where characteristic energies of  $\text{Na}_2\text{SO}_4$  and  $\text{Na}_2\text{O}$  are presented. Figure S.9d illustrates the Mg 2p spectrum, elucidating its presence in NSW. For instance, energies of 51.6, 50.4, and 49.3 eV correspond to  $\text{MgSO}_4$ ,  $\text{MgO}$ , and  $\text{Mg}(\text{OH})_2$ , respectively, compounds that can precipitate from NSW at alkaline conditions.

The use of  $\text{Na}_2\text{S}/\text{Na}_2\text{SO}_3$  as sacrificial agent in SSW experiments contributed significantly to increase the solution pH to highly alkaline values around  $12.7 \pm 0.2$ . Although alkaline conditions could benefit the water splitting reaction, excessive alkaline environment is not advantageous, because excessive hydroxide ions can react with hydrogen ions from water splitting reducing the hydrogen production efficiency [47]. However, as observed in Fig. 4, using NSW enhanced the photocatalytic activity due to the buffer capacity of the carbonate/bicarbonate pair that keeps the pH around  $10.0 \pm 0.2$ , which is more suitable for the photocatalytic reaction.

When  $\text{TiO}_2$  is present in SSW or UP, the initial pH value is  $5.9 \pm 0.2$ . However, the use of NSW increases the pH to  $8.4 \pm 0.2$  due to its buffer capacity, which is also advantageous for photocatalytic water splitting.

This increase in the HPR was also observed by Sakurai et al. [50] using Pt- $\text{TiO}_2$  with glycerol as sacrificial agent, achieving  $3000 \mu\text{mol h}^{-1} \text{g}_{\text{cat}}^{-1}$  in NSW and  $1400 \mu\text{mol h}^{-1} \text{g}_{\text{cat}}^{-1}$  in UP, due to the flocculation of the granules. But the trend observed in Fig. 4 differed to that reported by other authors, such as Zhu et al. [46], who worked with CdS/CDs, and lactic acid as sacrificial agent instead of  $\text{Na}_2\text{S}/\text{Na}_2\text{SO}_3$ . They observed worse photocatalytic activity in NSW compared to UP water and attributed the results to the ionic components of NSW, even though they did not mention the pH values. Ayyub et al. [52] reported worse performance for  $\text{TiO}_2/\text{Pt}/\text{Cd}_{0.8}\text{Zn}_{0.2}\text{S}$ , and  $\text{ZnO}/\text{Pt}/\text{Cd}_{0.8}\text{Zn}_{0.2}\text{S}$  in NSW with respect to UP when benzyl alcohol/acetic acid was used as sacrificial agent but the performance improved when  $\text{Na}_2\text{S}/\text{Na}_2\text{SO}_3$  was used as sacrificial agent. Ji et al. [49] did not observe a significant difference between NSW and UP, achieving 1860 and  $1660 \mu\text{mol h}^{-1} \text{g}_{\text{cat}}^{-1}$  with Pt-CdS/ $\text{TiO}_2$ , respectively. Similar observations were reported by Speltini et al. [51] with Pt-o-g- $\text{C}_3\text{N}_4$ , which obtained  $840 \mu\text{mol h}^{-1} \text{g}_{\text{cat}}^{-1}$  in both water media (NSW and UP).

The deep improvement observed in this work working with NSW underscores the critical role of considering operating conditions of real scenarios when designing and optimizing photocatalytic systems for sustainable hydrogen generation. Therefore, the hydrogen production using CdS as photocatalyst was analyzed under different operation conditions: as catalyst concentration, and sacrificial agent concentration.

Fig. 5 depicts the influence of the catalyst concentration. As seen in Fig. 5b, the accumulated hydrogen production is quite similar for concentrations of CdS from 25 to  $150 \text{ mg L}^{-1}$ , disclosing no need for high

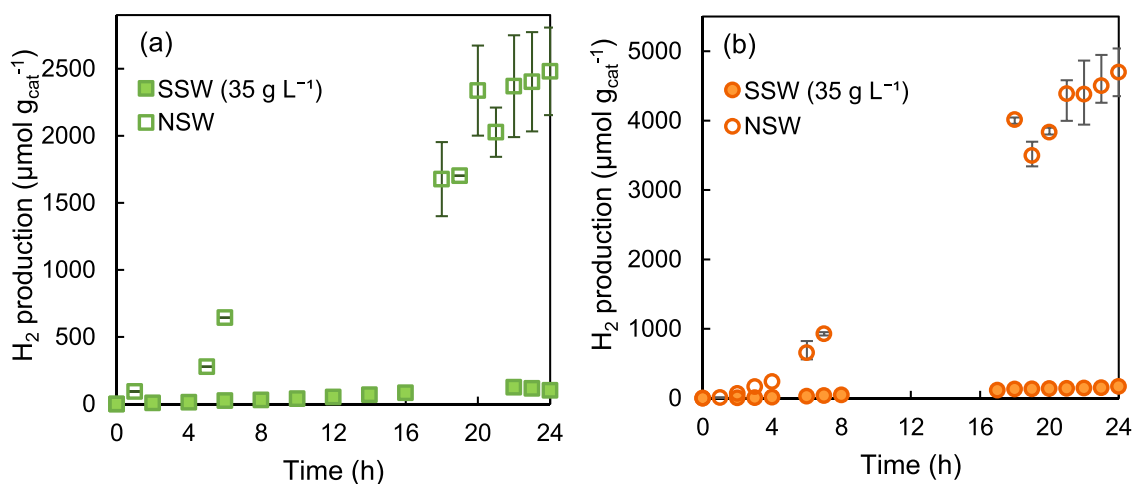


Fig. 4. Comparison in the  $\text{H}_2$  production between NSW and SSW ( $35 \text{ g L}^{-1}$  of NaCl) with (a)  $170 \text{ mg L}^{-1}$  of  $\text{TiO}_2$  with UV radiation and 20% of methanol and ( $100 \text{ mg L}^{-1}$  of CdS with visible light and 0.1 M of  $\text{Na}_2\text{S}/\text{Na}_2\text{SO}_3$ .

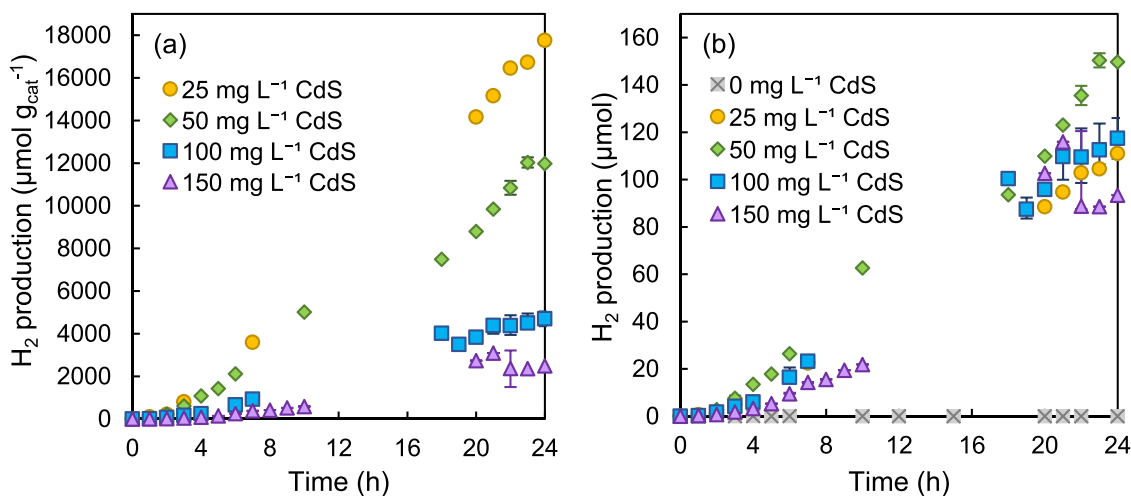


Fig. 5. Influence of the CdS concentration in the hydrogen production with NSW, visible light, and 0.1 M of Na<sub>2</sub>S/Na<sub>2</sub>SO<sub>3</sub>. (a) The hydrogen production per grams of catalyst, and (b) accumulated hydrogen production.

catalyst concentrations to improve the results. Using 50 mg L<sup>-1</sup> of CdS leads to the best performance for hydrogen production, with 0.1 M Na<sub>2</sub>S/Na<sub>2</sub>SO<sub>3</sub> as sacrificial agent and natural seawater. This is explained due to the shield effect that high CdS concentrations create in combination with the sacrificial agent in NSW (Figure S.11), which prevents light from reaching the surface of every particle of catalyst [46]. However, the blank experiment (Fig. 5b) without the addition of CdS revealed its necessity for photocatalytic hydrogen production. Negligible hydrogen production was observed without catalyst (Fig. 5b) and in dark conditions.

It is already known that the catalyst loading in the suspension could affect the physicochemical properties, such as adsorption and desorption with the reaction medium. Some authors have reported similar trends with respect to catalyst concentration. According to Lakshmana Reddy et al. [69], the optimal catalyst concentration for TiO<sub>2</sub> nanotubes was found to be 5 mg within the range of 3–100 mg. The same trend was observed for Cu<sub>2</sub>O catalyst, with optimal concentration of 0.05 g within the range of 0.1–1 g. This was due to the shield effect of the suspended particles, which reduced the light absorption of the photocatalyst above the optimal concentration. Rao et al. [4] showed that CuO/NiO@TiO<sub>2</sub> nanocomposite exhibited the highest hydrogen production with 20 mg of catalyst within a studied range from 5 to 100 mg.

In addition, the stability and the life-time of the photocatalyst are crucial in photocatalytic reactions. Therefore, five cycles of 5 h each

with CdS as catalyst were carried out to assess the catalyst stability (Fig. 6a). After every run, the reaction medium was purged with argon to remove the remaining air and the hydrogen produced in the experiment. As shown in Fig. 6a, the photocatalyst needs a few hours to activate before reaching its maximum hydrogen production, but afterwards the photocatalytic production rate is kept constant. Moreover, Fig. 6b shows results obtained in an experiment that lasted for almost one week. It is worth noting that the hydrogen production rate was  $3.9 \cdot 10^2 \mu\text{mol h}^{-1} \text{g}_{\text{cat}}^{-1}$  until 70 h, but decreased to  $2.7 \cdot 10^2 \mu\text{mol h}^{-1} \text{g}_{\text{cat}}^{-1}$  when the experiment was extended up to 152 h. These results reveal the potential of the proposed system.

Fig. 7 illustrates the effect of the sacrificial agent concentration. It shows that concentrations of Na<sub>2</sub>S/Na<sub>2</sub>SO<sub>3</sub> below 0.025 M are not enough, observing low rate of hydrogen production. A trade-off between the hydrogen production rate and the concentration of sacrificial agent is needed. Moreover, an increase in the concentration of sacrificial agent leads to an undesirable increase of the pH because it contributes to the formation of alkaline precipitates. Hence, in the studied range of sacrificial agent concentrations, 0.025 M of Na<sub>2</sub>S/Na<sub>2</sub>SO<sub>3</sub> is the most suitable concentration to achieve high hydrogen production rates. The hydrogen production is negligible when no sacrificial agent is used.

Simamora et al. [56] studied the influence of oxalic acid as sacrificial agent with CuO/nano-TiO<sub>2</sub> photocatalyst on the water and seawater splitting, and reported almost no influence in the range of

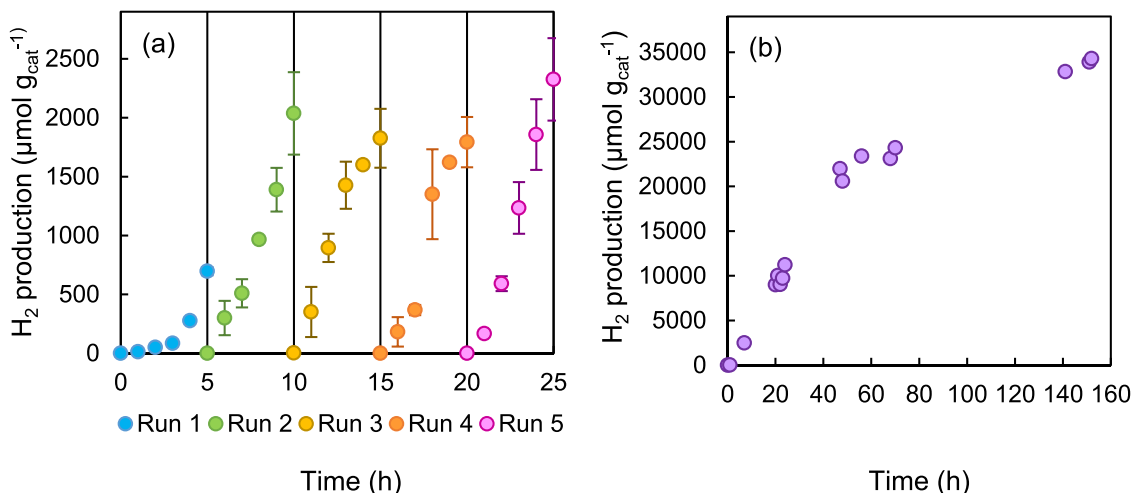


Fig. 6. CdS stability studies with 50 mg L<sup>-1</sup> of CdS, 0.1 M of Na<sub>2</sub>S/Na<sub>2</sub>SO<sub>3</sub>, NSW, and visible light, in (a) 5 runs of 5 hours, and (b) 152 h of experiment.

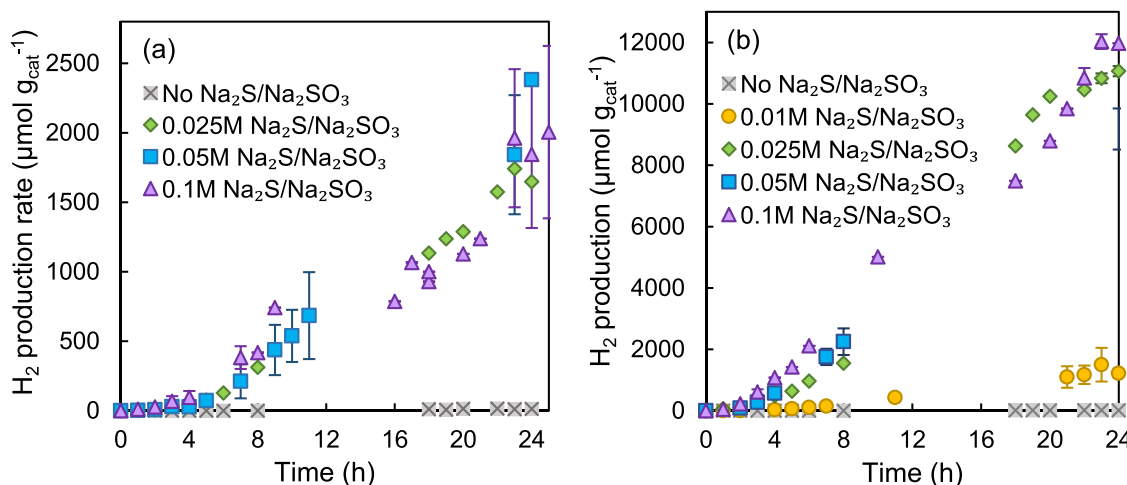


Fig. 7. Influence of the sacrificial agent concentration in the hydrogen production with NSW, visible light, and (a) 50 mg L<sup>-1</sup>, (b) 150 mg L<sup>-1</sup> of CdS.

0–50 mmol L<sup>-1</sup> of oxalic acid, and the negative influence of using excess of sacrificial agent. Ayyub et al. [52] evaluated the influence of different sacrificial agents in NSW with TiO<sub>2</sub>/Pt/Cd<sub>0.8</sub>Zn<sub>0.2</sub>S, and ZnO/Pt/Cd<sub>0.8</sub>Zn<sub>0.2</sub>S composites, observing different trends depending on the sacrificial agent. With Na<sub>2</sub>S/Na<sub>2</sub>SO<sub>3</sub> they observed better performance in NSW, and with benzyl alcohol/acetic acid in UP (Table S.1).

Based on the above experiments and analysis, it is concluded that the use of CdS as photocatalyst with Na<sub>2</sub>S/Na<sub>2</sub>SO<sub>3</sub> as sacrificial agent gives higher rates of hydrogen generation when working with NSW, compared to SSW. The carbonate/bicarbonate equilibrium, from NSW, acts as buffer making it possible to keep the pH around 10.0 ± 0.2, maximizing hydrogen production, besides the advantages of not working at an extreme alkaline pH.

This increase in the hydrogen production was also favored due to the regeneration of the photocatalyst by the sacrificial agent, following the Eqs. (18)–(22) [8].



The sacrificial agent, Na<sub>2</sub>S/Na<sub>2</sub>SO<sub>3</sub>, acts as hole scavenger in the catalyst's surface, being oxidized to S<sub>2</sub>O<sub>3</sub><sup>2-</sup>, as shown in Eq. (18).

Following the generation of hydroxyl radicals in the reaction medium helps understanding the mechanism of hydrogen production. It is noteworthy that the redox potential of H<sub>2</sub>O/·OH is ca. 2.3 V vs NHE. Therefore, only the VB of TiO<sub>2</sub> is more positive than the potential to generate ·OH, as demonstrated experimentally in Figure S.12.

The synergy between the use of Na<sub>2</sub>S/Na<sub>2</sub>SO<sub>3</sub> and NSW opens the door to new horizons where hydrogen can be obtained from CdS-based composites using an unlimited resource. The results obtained in batch mode of operation must be assessed in a continuous operation mode where the influence of variables and catalyst deactivation with time are analyzed.

#### 4. Conclusions

This study contributes to create essential knowledge towards harnessing photocatalytic hydrogen production in natural seawater, paving the way for the development of sustainable and efficient energy

conversion technologies. Previous articles referred to the use of seawater, both natural and simulated, for photocatalytic hydrogen generation show inconsistent data with no reliable conclusions, mainly attributed to the interactions of NaCl, which is the major salt, with the photocatalytic system. However, in this research, after having evaluated synthetic and natural seawater as water source, other compounds are found to be key to hydrogen production. This is the case of the carbonate/bicarbonate pair, whose chemical equilibrium causes a buffer effect that maintains the pH around 10.0 ± 0.2 when Na<sub>2</sub>S/Na<sub>2</sub>SO<sub>3</sub> is used as sacrificial agent, thus achieving higher hydrogen production compared to a similar system using synthetic seawater water.

Besides, this research assesses the influence of different operating parameters in the production of hydrogen. This investigation determined the influence of the CdS concentration, revealing no influence for concentrations above 50 mg L<sup>-1</sup> due to the shield effect exerted by the catalyst particles. The analysis of the influence of the concentration of the sacrificial agent demonstrated that it can be reduced down to 0.025 mol L<sup>-1</sup> without affecting the hydrogen production.

Furthermore, SEM and EDS analysis revealed the homogeneity of synthesized CdS versus commercial CdS. XPS analysis on the used materials confirmed the presence of the salts that precipitate on the surface of the photocatalyst due to the alkaline conditions, explaining the effect of different salts and ions contained in NSW. The improvement observed with CdS in NSW underscores the critical role of considering real scenarios operating conditions when designing and optimizing photocatalytic systems for sustainable hydrogen generation based on abundant and inexpensive raw materials. As it continues to unlock the tremendous promise of natural seawater, this advancement propels closer to realizing a greener and more environmentally friendly future powered by hydrogen energy.

#### CRediT authorship contribution statement

**María J. Rivero:** Conceptualization, Methodology, Project administration, Supervision, Writing – review & editing. **Inmaculada Ortiz:** Conceptualization, Funding acquisition, Supervision, Writing – review & editing. **Deva Pelayo:** Data curation, Investigation, Writing – original draft, Writing – review & editing. **Eduardo Pérez-Peña:** Data curation, Investigation, Writing – review & editing.

#### Declaration of Competing Interest

The authors declare that they have no known competing financial interests or personal relationships that could have appeared to influence the work reported in this paper.

## Data Availability

The data that has been used is confidential.

## Acknowledgements

These results are part of the R&D projects PLEC2021-007718 and PDC2022-133563-I00 funded by MCIN/AEI/10.13039/501100011033 and European Union NextGenerationEU/PRTR.

## Appendix A. Supporting information

Supplementary data associated with this article can be found in the online version at [doi:10.1016/j.cattod.2024.114672](https://doi.org/10.1016/j.cattod.2024.114672).

## References

- [1] S. Hilliard, "Water splitting photoelectrocatalysis: the conception and construction of a photoelectrocatalytic water splitting cell," 2016.
- [2] Y. Liu, et al., Photocatalytic hydrogen evolution using ternary-metal-sulfide/TiO<sub>2</sub> heterojunction photocatalysts, *ChemCatChem* vol. 14 (5) (2022), <https://doi.org/10.1002/cctc.202101439>.
- [3] F. Dingenen, S.W. Verbruggen, Tapping hydrogen fuel from the ocean: A review on photocatalytic, photoelectrochemical and electrolytic splitting of seawater, *Renew. Sustain. Energy Rev.* vol. 142 (2021) 110866, <https://doi.org/10.1016/j.rser.2021.110866>.
- [4] V. Navakoteswara Rao, et al., Metal chalcogenide-based core/shell photocatalysts for solar hydrogen production: recent advances, properties and technology challenges, *J. Hazard. Mater.* vol. 415 (2021) 125588, <https://doi.org/10.1016/j.jhazmat.2021.125588>.
- [5] R. Figaj, L. Vanoli, Hybrid and novel solar hydrogen systems, *Sol. Hydrog. Prod. Process. Syst. Technol.* (2019) 487–510, <https://doi.org/10.1016/B978-0-12-814853-2.00013-8>.
- [6] S. Ichikawa, Photoelectrocatalytic production of hydrogen from natural seawater under sunlight, *Int. J. Hydrog. Energy* vol. 22 (7) (1997) 675–678.
- [7] Y. Yao, X. Gao, X. Meng, Recent advances on electrocatalytic and photocatalytic seawater splitting for hydrogen evolution, *Int. J. Hydrog. Energy* vol. 46 (13) (2021) 9087–9100, <https://doi.org/10.1016/j.ijhydene.2020.12.212>.
- [8] J.A. Nasir, Z.U. Rehman, S.N.A. Shah, A. Khan, I.S. Butler, C.R.A. Catlow, Recent developments and perspectives in CdS-based photocatalysts for water splitting, *J. Mater. Chem. A* vol. 8 (40) (2020) 20752–20780, <https://doi.org/10.1039/d0ta05834c>.
- [9] A. Fujishima, K. Honda, Electrochemical photolysis of water at a semiconductor electrode, *Nature* vol. 238 (1972) 37–38.
- [10] J. Corredor, D. Harankahage, F. Gloaguen, M.J. Rivero, M. Zamkov, I. Ortiz, Influence of QD photosensitizers in the photocatalytic production of hydrogen with biomimetic [FeFe]-hydrogenase. Comparative performance of CdSe and CdTe, *Chemosphere* vol. 278 (2021) 130485, <https://doi.org/10.1016/j.chemosphere.2021.130485>.
- [11] J. Corredor, M.J. Rivero, I. Ortiz, New insights in the performance and reuse of rGO/TiO<sub>2</sub> composites for the photocatalytic hydrogen production, *Int. J. Hydrog. Energy* vol. 46 (33) (2021) 17500–17506, <https://doi.org/10.1016/j.ijhydene.2020.01.181>.
- [12] P. Fernández-Castro, M. Vallejo, M.F. San Román, I. Ortiz, Insight on the fundamentals of advanced oxidation processes: role and review of the determination methods of reactive oxygen species, *J. Chem. Technol. Biotechnol.* vol. 90 (5) (2015) 796–820, <https://doi.org/10.1002/jctb.4634>.
- [13] X. Li, et al., Photocatalytic hydrogen production over CdS nanomaterials: an interdisciplinary experiment for introducing undergraduate students to photocatalysis and analytical chemistry, *J. Chem. Educ.* vol. 96 (6) (2019) 1224–1229, <https://doi.org/10.1021/acs.jchemed.9b00087>.
- [14] S.C. Zhu, F.X. Xiao, Transition metal chalcogenides quantum dots: emerging building blocks toward solar-to-hydrogen conversion, *ACS Catal.* vol. 13 (11) (2023) 7269–7309, <https://doi.org/10.1021/acscatal.2c05401>.
- [15] L. Zhang, et al., Research progress on synthetic and modification strategies of CdS-based photocatalysts, *Ionics* vol. 29 (6) (2023) 2115–2139, <https://doi.org/10.1007/s11581-023-05004-z>.
- [16] J. Corredor, M.J. Rivero, C.M. Rangel, F. Gloaguen, I. Ortiz, Comprehensive review and future perspectives on the photocatalytic hydrogen production, *J. Chem. Technol. Biotechnol.* vol. 94 (10) (2019) 3049–3063, <https://doi.org/10.1002/jctb.6123>.
- [17] S.S. Martín, M.J. Rivero, I. Ortiz, Unravelling the mechanisms that drive the performance of photocatalytic hydrogen production, *Catalysts* vol. 10 (8) (2020) 1–27, <https://doi.org/10.3390/catal10080901>.
- [18] I. Dincer, C. Zamfirescu, *Hydrog. Prod. Photon. Energy* vol. i. (2016).
- [19] D. DeepanPrakash, V. Premnath, C. Raghu, S. Vishnukumar, S.S. Jayanthi, D. Easwaramoorthy, Harnessing power from sea water using nano material as photocatalyst and solar energy as light source: the role of hydrocarbon as dual agent, *Int. J. Energy Res.* vol. 38 (2014) 249–253, <https://doi.org/10.1002/er>.
- [20] A. García Sánchez, Desarrollo de Catalizadores Híbridos Multifuncionales para la Producción de Combustibles Solares, 2023.
- [21] S. Liu, et al., Hollow heterostructure CoS/CdS photocatalysts with enhanced charge transfer for photocatalytic hydrogen production from seawater, *Int. J. Hydrog. Energy* vol. 47 (15) (2022) 9220–9229, <https://doi.org/10.1016/j.ijhydene.2021.12.259>.
- [22] M.J. Rivero, O. Iglesias, P. Ribao, I. Ortiz, Kinetic performance of TiO<sub>2</sub>/Pt/reduced graphene oxide composites in the photocatalytic hydrogen production, *Int. J. Hydrog. Energy* vol. 44 (1) (2019) 101–109, <https://doi.org/10.1016/j.ijhydene.2018.02.115>.
- [23] P. Makula, M. Pacia, W. Macyk, How to correctly determine the band gap energy of modified semiconductor photocatalysts based on UV-Vis spectra, *J. Phys. Chem. Lett.* vol. 9 (23) (2018) 6814–6817, <https://doi.org/10.1021/acs.jpclett.8b02892>.
- [24] F. Fresno, O. Iglesias, E. Alfonso-González, M.J. Rivero, I. Ortiz, V.A. de la Peña O'Shea, Assessing the feasibility of reduced graphene oxide as an electronic promoter for photocatalytic hydrogen production over Nb-Ta perovskite photocatalysts, *Catal. Today* vol. 362 (2021) 22–27, <https://doi.org/10.1016/j.cattod.2020.05.027>.
- [25] M. Gao, P.K.N. Connor, G.W. Ho, Plasmonic photothermic directed broadband sunlight harnessing for seawater catalysis and desalination, *Energy Environ. Sci.* vol. 9 (10) (2016) 3151–3160, <https://doi.org/10.1039/c6ee00971a>.
- [26] L. Guo, et al., MoS<sub>2</sub>/TiO<sub>2</sub> heterostructures as nonmetal plasmonic photocatalysts for highly efficient hydrogen evolution, *Energy Environ. Sci.* vol. 11 (1) (2018) 106–114, <https://doi.org/10.1039/c7ee02464a>.
- [27] L. Xia, Y. Lu, Y.Z. Li, Z.Y. Hu, X.Y. Yang, TiO<sub>2</sub>-rGO-Cu complex: A photocatalyst possessing an interfacial electron transport mechanism to enhance hydrogen production from seawater, *Chem. Phys. Lett.* vol. 822 (2023), <https://doi.org/10.1016/j.cplett.2023.140498>.
- [28] V. Kumaravel, et al., Photocatalytic hydrogen production: Role of sacrificial reagents on the activity of oxide, carbon, and sulfide catalysts, *Catalysts* vol. 9 (3) (2019), <https://doi.org/10.3390/catal9030276>.
- [29] M. Wang, S. Shen, L. Li, Z. Tang, J. Yang, Effects of sacrificial reagents on photocatalytic hydrogen evolution over different photocatalysts, *J. Mater. Sci.* vol. 52 (9) (2017) 5155–5164, <https://doi.org/10.1007/s10853-017-0752-z>.
- [30] J. Corredor, E. Perez-Peña, M.J. Rivero, I. Ortiz, Performance of rGO/TiO<sub>2</sub> photocatalytic membranes for hydrogen production, *Membranes* vol. 10 (9) (2020) 1–13, <https://doi.org/10.3390/membranes10090218>.
- [31] T. Li, N. Tsubaki, Z. Jin, S-scheme heterojunction in photocatalytic hydrogen production, *J. Mater. Sci. Technol.* vol. 169 (2024) 82–104, <https://doi.org/10.1016/j.jmst.2023.04.049>.
- [32] F. Jamal, et al., Review of metal sulfide nanostructures and their applications, *ACS Appl. Nano Mater.* vol. 6 (9) (2023) 7077–7106, <https://doi.org/10.1021/acsnm.3c00417>.
- [33] L. Zhang, et al., Ternary CdS@MoS<sub>2</sub>-Co<sub>3</sub>O<sub>4</sub> multiheterojunction photocatalyst for boosting photocatalytic H<sub>2</sub> evolution, *ACS Appl. Mater. Interfaces* vol. 15 (37) (2023) 43790–43798, <https://doi.org/10.1021/acsmi.3c09073>.
- [34] S.K. Nadikatla, V.B. Chintada, T.R. Gurugubelli, R. Koutavarapu, Review of recent developments in the fabrication of ZnO/CdS heterostructure photocatalysts for degradation of organic pollutants and hydrogen production, *Molecules* vol. 28 (11) (2023), <https://doi.org/10.3390/molecules28114277>.
- [35] S. Shaheen, S.A. Ali, U.F. Mir, I. Sadiq, T. Ahmad, Recent advances in transition metal phosphide nanocatalysts for H<sub>2</sub> evolution and CO<sub>2</sub> reduction, *Catalysts* vol. 13 (7) (2023), <https://doi.org/10.3390/catal13071046>.
- [36] P.O. Fadojutimi, S.S. Gqoba, Z.N. Tetana, J. Moma, Transition metal dichalcogenides [MX<sub>2</sub>] in photocatalytic water splitting, *Catalysts* vol. 12 (5) (2022), <https://doi.org/10.3390/catal12050468>.
- [37] X. Ning, G. Lu, Photocorrosion inhibition of CdS-based catalysts for photocatalytic overall water splitting, *Nanoscale* vol. 12 (3) (2020) 1213–1223, <https://doi.org/10.1039/c9nr09183a>.
- [38] M. Tahir, S. Tasleem, B. Tahir, Recent development in band engineering of binary semiconductor materials for solar driven photocatalytic hydrogen production, *Int. J. Hydrog. Energy* vol. 45 (32) (2020) 15985–16038, <https://doi.org/10.1016/j.ijhydene.2020.04.071>.
- [39] S.G. Kumar, R. Kavitha, P.M. Nithya, Tailoring the CdS surface structure for photocatalytic applications, *J. Environ. Chem. Eng.* vol. 8 (5) (2020) 104313, <https://doi.org/10.1016/j.jece.2020.104313>.
- [40] X. Luo, et al., Tandem CdS/TiO<sub>2</sub>(B) nanosheet photocatalysts for enhanced H<sub>2</sub> evolution, *Appl. Surf. Sci.* vol. 515 (2020) 145970, <https://doi.org/10.1016/j.apsusc.2020.145970>.
- [41] D. He, et al., Enhanced cyclability of CdS/TiO<sub>2</sub> photocatalyst by stable interface structure, *Superlattices Microstruct.* vol. 51 (6) (2012) 799–808, <https://doi.org/10.1016/j.spmi.2012.03.026>.
- [42] X. Yue, S. Yi, R. Wang, Z. Zhang, S. Qiu, Cadmium sulfide and nickel synergetic catalysts supported on graphitic carbon nitride for visible-light-driven photocatalytic hydrogen evolution, *Sci. Rep.* vol. 6 (1) (2016) 9, <https://doi.org/10.1038/srep22268>.
- [43] Y. Zhu, et al., Visible light induced photocatalysis on CdS quantum dots decorated TiO<sub>2</sub> nanotube arrays, *Appl. Catal. A Gen.* vol. 498 (2015) 159–166, <https://doi.org/10.1016/j.apcata.2015.03.035>.
- [44] H. Wang, J. Li, H. Zhou, S. Yao, W. Zhang, Template synthesis and characterization of CdS/TiO<sub>2</sub> coaxial nanocables for photocatalysis in visible light, *J. Mater. Sci. Mater. Electron.* vol. 30 (11) (2019) 10754–10764, <https://doi.org/10.1007/s10854-019-01419-5>.
- [45] X.L. Wang, R.R. Zheng, H. Yu, X.T. Dong, Preparation and photocatalytic hydrogen production properties of mesoporous CdS/TiO<sub>2</sub> composites, *Nano* vol. 15 (2) (2020) 1–8, <https://doi.org/10.1142/S1793292020500198>.

- [46] C. Zhu, et al., Construction of CDs/CdS photocatalysts for stable and efficient hydrogen production in water and seawater, *Appl. Catal. B Environ.* vol. 242 (2019) 178–185, <https://doi.org/10.1016/j.apcatb.2018.09.096>.
- [47] Y.C. Chang, Y.R. Lin, Construction of Ag/Ag<sub>2</sub>S/CdS heterostructures through a facile two-step wet chemical process for efficient photocatalytic hydrogen production, *Nanomaterials* vol. 13 (12) (2023), <https://doi.org/10.3390/nano13121815>.
- [48] Drugbank Online, Sodium sulfide, 2023. (<https://go.drugbank.com/drugs/DB11159>).
- [49] S.M. Ji, H. Jun, J.S. Jang, H.C. Son, P.H. Borse, J.S. Lee, Photocatalytic hydrogen production from natural seawater, *J. Photochem. Photobiol. A Chem.* vol. 189 (1) (2007) 141–144, <https://doi.org/10.1016/j.jphotochem.2007.01.011>.
- [50] H. Sakurai, M. Kiuchi, T. Jin, Pt/TiO<sub>2</sub> granular photocatalysts for hydrogen production from aqueous glycerol solution: durability against seawater constituents and dissolved oxygen, *Catal. Commun.* vol. 114 (2018) 124–128, <https://doi.org/10.1016/j.catcom.2018.06.013>.
- [51] A. Speltini, et al., Improved photocatalytic H<sub>2</sub> production assisted by aqueous glucose biomass by oxidized g-C<sub>3</sub>N<sub>4</sub>, *Int. J. Hydrog. Energy* vol. 43 (32) (2018) 14925–14933, <https://doi.org/10.1016/j.ijhydene.2018.06.103>.
- [52] M.M. Ayyub, M. Chhetri, U. Gupta, A. Roy, C.N.R. Rao, Photochemical and Photoelectrochemical Hydrogen Generation by Splitting Seawater, *Chem. Eur. J.* vol. 24 (69) (2018) 18455–18462, <https://doi.org/10.1002/chem.201804119>.
- [53] C. Tai, J.F. Peng, J.F. Liu, G. Bin Jiang, H. Zou, Determination of hydroxyl radicals in advanced oxidation processes with dimethyl sulfoxide trapping and liquid chromatography, *Anal. Chim. Acta* vol. 527 (2004) 73–80, <https://doi.org/10.1016/j.aca.2004.08.019>.
- [54] B. Bajorowicz, A. Cybula, M.J. Winiarski, T. Klimczuk, A. Zaleska, Surface properties and photocatalytic activity of KTaO<sub>3</sub>, CdS, MoS<sub>2</sub> semiconductors and their binary and ternary semiconductor composites, *Molecules* vol. 19 (9) (2014) 15339–15360, <https://doi.org/10.3390/molecules190915339>.
- [55] B. Han, Y.H. Hu, MoS<sub>2</sub> as a co-catalyst for photocatalytic hydrogen production from water, *Energy Sci. Eng.* vol. 4 (5) (2016) 285–304, <https://doi.org/10.1002/ese3.128>.
- [56] A.J. Simamora, F.C. Chang, H.P. Wang, T.C. Yang, Y.L. Wei, W.K. Lin, H<sub>2</sub> fuels from photocatalytic splitting of seawater affected by nano-TiO<sub>2</sub> promoted with CuO and NiO, *Int. J. Photoenergy* vol. 2013 (2013) 1–6, <https://doi.org/10.1155/2013/419182>.
- [57] A.J. Simamora, T.L. Hsiung, F.C. Chang, T.C. Yang, C.Y. Liao, H.P. Wang, Photocatalytic splitting of seawater and degradation of methylene blue on CuO/nano TiO<sub>2</sub>, *Int. J. Hydrog. Energy* vol. 37 (18) (2012) 13855–13858, <https://doi.org/10.1016/j.ijhydene.2012.04.091>.
- [58] H. Che, G. Che, E. Jiang, C. Liu, H. Dong, C. Li, A novel Z-Scheme CdS/Bi<sub>2</sub>O<sub>4</sub>Cl heterostructure for photocatalytic degradation of antibiotics: Mineralization activity, degradation pathways and mechanism insight, *J. Taiwan Inst. Chem. Eng.* vol. 91 (2018) 224–234, <https://doi.org/10.1016/j.jtice.2018.05.004>.
- [59] H.L. Lee, A.M. Issam, M. Belmahi, M.B. Assouar, H. Rinnert, M. Alnot, Synthesis and characterizations of bare cds nanocrystals using chemical precipitation method for photoluminescence application, *J. Nanomater.* (2009), <https://doi.org/10.1155/2009/914501>.
- [60] S. Liu, Z. Guo, X. Qian, J. Zhang, J. Liu, J. Lin, Sonochemical deposition of ultrafine metallic Pt nanoparticles on CdS for efficient photocatalytic hydrogen evolution, *Sustain. Energy Fuels* vol. 3 (4) (2019) 1048–1054, <https://doi.org/10.1039/C9SE00050J>.
- [61] L. Wu, J.C. Yu, X. Fu, Characterization and photocatalytic mechanism of nanosized CdS coupled TiO<sub>2</sub> nanocrystals under visible light irradiation, *J. Mol. Catal. A Chem.* vol. 244 (1–2) (2006) 25–32, <https://doi.org/10.1016/j.molcata.2005.08.047>.
- [62] M. Sonaimuthu, et al., Multiple heteroatom dopant carbon dots as a novel photoluminescent probe for the sensitive detection of Cu<sup>2+</sup> and Fe<sup>3+</sup> ions in living cells and environmental sample analysis, *Environ. Res.* vol. 219 (2023) 115106, <https://doi.org/10.1016/j.envres.2022.115106>.
- [63] S. Mohandoss, et al., Multicolor emission-based nitrogen, sulfur and boron co-doped photoluminescent carbon dots for sequential sensing of Fe<sup>3+</sup> and cysteine: RGB color sensor and live cell imaging, *Spectrochim. Acta Part A Mol. Biomol. Spectrosc.* vol. 302 (2023) 123040, <https://doi.org/10.1016/j.saa.2023.123040>.
- [64] “XPS fitting, 2021. (<http://www.xpsfitting.com/>).
- [65] A.V. Naumkin, A. Kraust-Vass, S.W. Gaarenstroom, and C.J. Powell, NIST X-ray Photoelectron Spectroscopy Database, 2012. (<https://srdata.nist.gov/xps/>).
- [66] R. Benoit, LaSurface, CNRS Orléans. (<http://www.lasurface.com/accueil/>).
- [67] M. Krivec, R. Dillert, D.W. Bahnemann, A. Mehle, J. Štrancar, G. Dražić, The nature of chlorine-inhibition of photocatalytic degradation of dichloroacetic acid in a TiO<sub>2</sub>-based microreactor, *Phys. Chem. Chem. Phys.* vol. 16 (28) (2014) 14867–14873, <https://doi.org/10.1039/c4cp01043d>.
- [68] J. Lu, et al., Photothermal effect of carbon dots for boosted photothermal-assisted photocatalytic water/seawater splitting into hydrogen, *Chem. Eng. J.* vol. 453 (2023) 139834, <https://doi.org/10.1016/j.cej.2022.139834>.
- [69] N. Lakshmana Reddy, et al., Nanostructured semiconducting materials for efficient hydrogen generation, *Environ. Chem. Lett.* vol. 16 (3) (2018) 765–796, <https://doi.org/10.1007/s10311-018-0722-y>.